

Research Article

Diffusion-Controlled Synthesis of Magnetic Nanoparticles

David Heinke^{a,*} · Nicole Gehrke^a · Daniel Schmidt^b · Uwe Steinhoff^b · Thilo Viereck^c · Hilke Remmer^c · Frank Ludwig^c · Mihály Pósfai^d · Andreas Briel^a

^ananoPET Pharma GmbH, Berlin, Germany

^bPhysikalisch-Technische Bundesanstalt, Berlin, Germany

^cInstitute of Electrical Measurement and Fundamental Electrical Engineering, Technical University Braunschweig, Braunschweig, Germany

^dDepartment of Earth and Environmental Sciences, University of Pannonia, Veszprém, Hungary

*Corresponding author, email: david.heinke@nanopet.de

Received 27 November 2015; Accepted 22 February 2016; Published online 21 March 2016

© 2016 Heinke; licensee Infinite Science Publishing GmbH

This is an Open Access article distributed under the terms of the Creative Commons Attribution License (<http://creativecommons.org/licenses/by/4.0>), which permits unrestricted use, distribution, and reproduction in any medium, provided the original work is properly cited.

Abstract

Technological advancements of the Magnetic Particle Imaging (MPI) scanner and image reconstruction are important steps in the process of bringing MPI to preclinical and clinical applications. The future of this promising imaging modality, however, also crucially relies on the development of MPI tracers with high performance. An interesting material, not only for MPI, encompasses biogenic iron oxide nanoparticles due to their superior magnetic properties. It is a fact, however, that the production of such particles is extremely challenging. A promising approach for their manufacture is through the application of biomimetic synthesis routes. In the present study, a diffusion-controlled synthesis of magnetic nanoparticles, mimicking certain aspects of biomineralization *in vitro* is presented. The particles' structural as well as static and dynamic magnetic properties are characterized and their potential as an MPI tracer is investigated.

1. Introduction

Magnetic iron oxide nanoparticles are numbered among the most suitable materials for the development of MPI tracers. Indeed, new iron oxide particles have been synthesized exhibiting Magnetic Particle Spectra (MPS) wherein the amplitudes of the harmonics exceed that of the former gold standard, Resovist[®] [1–3]. Since Resovist is no longer commercially available, FeraSpin[™] R, which has been shown to exhibit MPS properties similar to Resovist [4], is used as a reference material in the field of tracer research with increasing frequency. Some of the highest MPI efficacies found so far were observed in experimental results for biogenic magnetite nanoparticles synthe-

sized by magnetotactic bacteria via biomineralization [5]. These nanoparticles consist of pure and almost defect-free monocrystalline magnetite of distinctive monodispersity in size and shape stabilized by biomembranes [6]. All these features seem to be ideal preconditions for the application of biogenic magnetite nanoparticles as tracers in MPI. However, since the production of larger amounts of such particles is technically challenging, current research focuses on biomimetic synthesis routes, which aim at mimicking biomineralization pathways *in vitro* [7].

In this work, we present a modification of the basic coprecipitation reaction, which takes place in a hydrogel network. This synthesis approach offers control over

crystal growth by decreasing the diffusion rates of the reactants as well as by suppressing convection [8]. In this way, we aim to model important parameters of biomineralization *in vitro*, namely the controlled crystallization in defined compartments.

II. Material and Methods

II.I. Nanoparticle Synthesis

Ferrous chloride hexahydrate ($\text{FeCl}_3 \cdot 6\text{H}_2\text{O}$), ferric chloride tetrahydrate ($\text{FeCl}_2 \cdot 4\text{H}_2\text{O}$) and sodium hydroxide (NaOH) were purchased from Sigma-Aldrich. Nitric acid (HNO_3 , 65 %) and hydrogen peroxide (H_2O_2 , 30 %) were purchased from Carl Roth. All chemicals were used as supplied. Ultrapure water with a conductivity less than $0.055 \mu\text{S}/\text{cm}$ was used for the preparation of all solutions.

Diffusion-controlled synthesis of magnetic nanoparticles was carried out according to [9] with minor modifications. In short, a 1:2 molar ratio solution of ferrous and ferric ions was added to an agarose gel prepared in ultrapure water. Over a period of 24 h, the ferrous and ferric ions were allowed to diffuse into the gel. After washing with ultrapure water a NaOH solution was carefully added to the gel. A thin black layer occurred immediately after NaOH addition, indicating the formation of iron oxide nanoparticles. The sample was left to stand at room temperature for several hours and subsequently, the iron oxide was separated from the gel, followed by repeated washing with ultrapure water. Thereafter, the resultant black slurry was treated with nitric acid and washed again with ultrapure water resulting in a dispersion of colloiddally stable magnetic nanoparticles NPIO-105.

II.II. Nanoparticle Characterization

The mean intensity-weighted hydrodynamic diameter of the particles was determined by dynamic light scattering using a NICOMP Submicron Particle Sizer Model 370 (NICOMP Particle Sizing Systems). The morphology and crystal sizes were investigated by transmission electron microscopy (TEM) using a Tecnai G2 Spirit BioTWIN (FEI). High-resolution TEM (HR-TEM) images were recorded with a JEOL JEM 3010. A Zetasizer nano ZS (Malvern) was used for the determination of the zeta-potential.

To estimate the particles' performance as potential MPI tracers, their MPS was recorded at a drive field with an amplitude of $10 \text{ mT}/\mu_0$ and a frequency, $f_0 = 25 \text{ kHz}$ using a commercial MPS system (Bruker BioSpin). The effective magnetic core sizes were estimated via static magnetization measurements using an MPMS XL (Quantum Design). Magnetorelaxometry (MRX) measurements were conducted by magnetizing the particles at a field of

2 mT amplitude for a duration of 2 sec and recording the loss of its magnetization over a period of 1.5 sec.

III. Results

III.I. Physicochemical Characterization

The particles synthesized here exhibit a mean hydrodynamic diameter of about 55 nm. The positive zeta-potential of +47 mV at a pH of 4.2 is caused by the acid treatment and the resulting protonated particle surface and indicates a colloidal stabilization via electrostatic repulsion.

From TEM micrographs (see example in Fig. 1), a mean crystallite size of 24 nm and a standard deviation of 10 nm was determined by measuring the horizontal Feret's diameter at different magnifications. The electron diffraction pattern proves the iron oxide phase of the particles to be cubic $\text{Fe}_3\text{O}_4/\gamma\text{-Fe}_2\text{O}_3$ (magnetite/maghemite) (Fig. 1 inset).

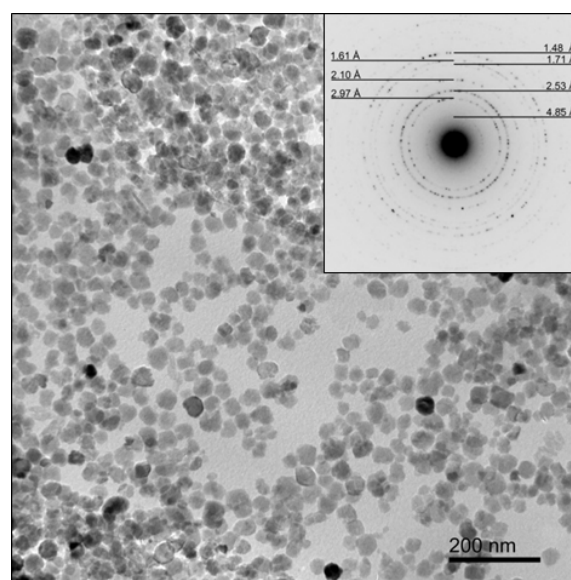


Figure 1: TEM micrograph of NPIO-105 synthesized via controlled coprecipitation and electron diffraction pattern being characteristic for magnetite/maghemite (inset).

In the TEM image the irregular outlines of the particles as well as their inhomogeneous image contrast suggest that the particles are composed of several small crystallites. However, high-resolution TEM images (see example in Fig. 2) reveal continuous lattice fringes over the entire particles and consequently imply that most of the particles behave like single crystals. This might be attributed to a mechanism of nucleation and growth as described by Baumgartner et al. [10]. Here, the growth of slowly precipitated magnetite nanoparticles in aqueous solution occurred by aggregation and coalescence of primary particles of about 2 nm.

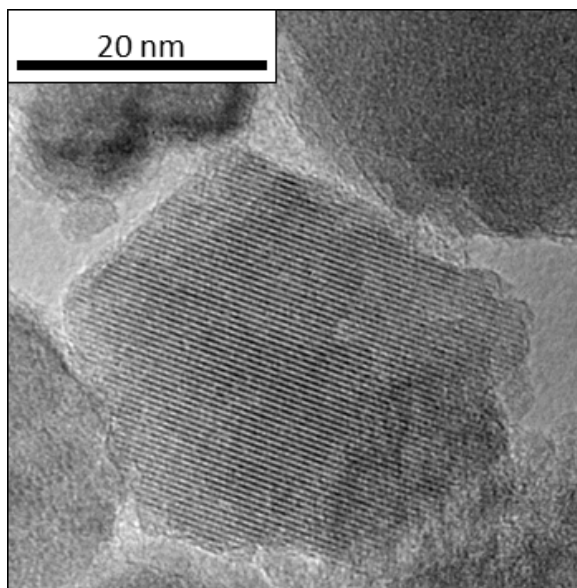


Figure 2: Typical high-resolution TEM micrograph of NPIO-105 synthesized via controlled coprecipitation.

III.II. Magnetic Particle Spectroscopy

The MPS of NPIO-105 and FeraSpin R (for comparison) are shown in Fig. 3.

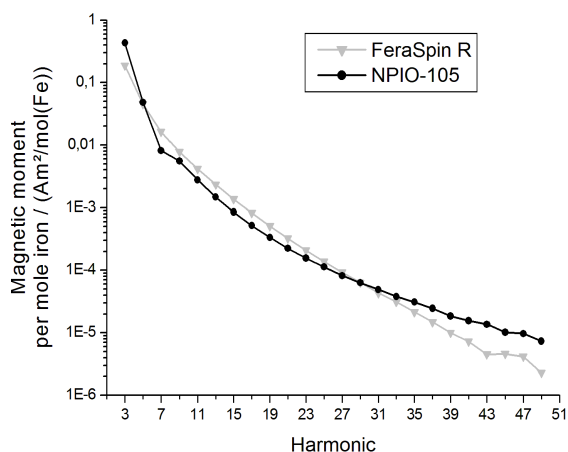


Figure 3: MPS of NPIO-105 and FeraSpin R measured at 10 mT/ μ_0 and $f_0 = 25$ kHz.

The third harmonic of the MPS of NPIO-105 exceeds that of the benchmark FeraSpin R by a factor of 2.3. However, the steep amplitude decay causes less intense harmonics to be observed as from harmonic number 7. This may be attributed to interparticle magnetic interactions, especially considering the absence of a protective polymeric coating, as well as the incapability of their magnetic moments to follow the sinusoidal excitation field of 25 kHz due to their large crystal size. Surprisingly, at

higher harmonics (from harmonic number 21 onwards), the decay becomes less steep causing similar signal intensities compared to FeraSpin R. At even higher harmonics (from harmonic number 29), the MPS intensity of NPIO-105 exceeds again that of FeraSpin R.

III.III. Static Magnetization

The initial magnetization of the particles' dispersion was measured (Fig. 4 inset) and used for the estimation of the effective magnetic core size distribution, assuming single domain spheres. The effective magnetic core size distribution of NPIO-105 was estimated from the best fit of a bimodal size distribution $f = (1 - \beta_2)f_1 + \beta_2f_2$ where f_1 and f_2 are lognormal functions (Fig. 4). As shown in [4], the MPS signal mainly arises from the second magnetic size mode. Comparing the core size distributions of NPIO-105 with FeraSpin R, the volume fraction f_2 of the former is significantly larger, while simultaneously being in the theoretically predicted ideal size range for MPI of 30 nm [10]. Thus, one could expect significantly higher MPS signal intensities for NPIO-105. However, it must be noted that the $M(H)$ measurement is a quasistatic method, which does not consider particle dynamics, and consequently cannot completely predict the particles' MPS performance.

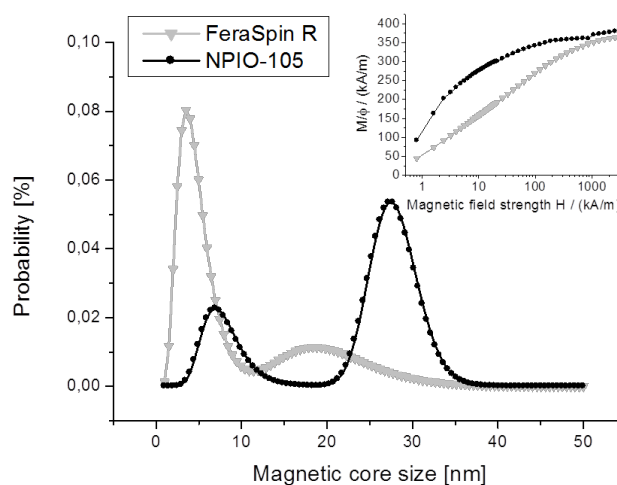


Figure 4: Distribution of the effective magnetic core size of NPIO-105 and FeraSpin R obtained from their initial $M(H)$ -curves (inset) normalized to the volume fraction of magnetite.

III.IV. Magnetorelaxometry

Magnetorelaxometric measurements were performed on suspended as well as on immobilized particles. Prior to switching of the magnetic field, the magnetization of the mobile sample is much higher than that of the immobilized sample (Fig. 5 inset). This is a result of the suppression of complete particle rotation due to the immo-

bilization process. Thus, the magnetic reorientation can only occur via the Néel process, while in the suspended state both Néel and Brownian rotation are present. The difference in the magnetization levels reveals that the majority of the particles relax via the Brownian process.

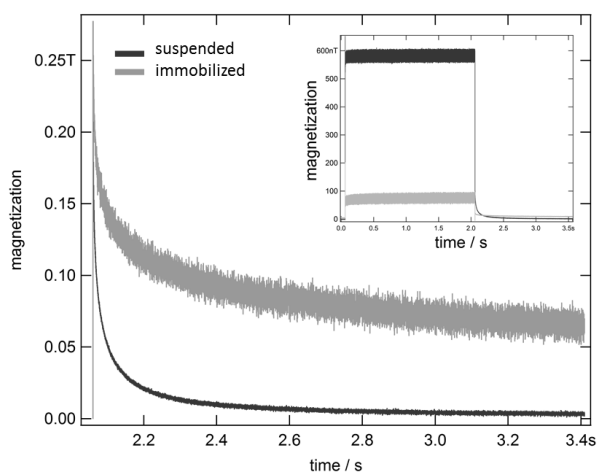


Figure 5: MRX curves of NPIO-105 in suspended and in immobilized state normalized to the signal intensity prior to switching of the magnetic field and initial MRX curves (inset).

Another indication for large magnetic cores is the long relaxation time of the immobilized sample in Fig. 5, depicting the MRX curves normalized to the magnetization detected prior to switching of the magnetic field. The long Néel time constant as well as the Brownian-dominated relaxation of the particle system probably accounts for the steep decay of the MPS, since a significant proportion of the particles' magnetic moments cannot follow the excitation field of 25 kHz and consequently do not contribute to the MPS signal.

IV. Conclusion

In this work, magnetic nanoparticles were synthesized by a controlled coprecipitation process via gel diffusion, mimicking important parameters of biomineralization *in vitro*. Their physicochemical and magnetic properties were thoroughly characterized. In contrast to the alkaline coprecipitation performed in solution, in which the crystal size can be tailored in the range of about 2–17 nm [11], the synthesis in a hydrogel network resulted in significantly larger mean crystallite sizes of 24 nm. Furthermore, the particle cores exhibit interesting morphologies being atypical for coprecipitated particles. As determined from static magnetization, the dispersion exhibits a large fraction of particles with effective magnetic core sizes of about 28 nm. Thus, the presented method enables the synthesis of magnetic nanoparticles with magnetic core sizes within the ideal size range for MPI. However, relaxation effects may cause a significant signal loss.

Future work will involve the steric stabilization of the particles via polymeric coatings, in order to reduce inter-particle magnetic interactions and thus to enhance the MPS signal intensities by minimizing relaxation effects. In addition, the influence of various synthesis parameters, such as the viscosity and the pore size of the gel, will be analysed in more detail in order to optimize the MPI performance of the particles.

Acknowledgments

This work was supported by the European Commission Framework Programme 7 under the NanoMag project [grant agreement no 604448] and the DFG priority program SPP1681 (LU800/4-1).

References

- [1] N. Gehrke, D. Heinke, D. Eberbeck, F. Ludwig, T. Wawrzik, C. Kuhlmann, and A. Briel. Magnetic characterization of clustered core magnetic nanoparticles for mpi. *IEEE Trans. Magn.*, 51(2):1–4, 2015. doi:10.1109/TMAG.2014.2358275.
- [2] K. Lütke-Buzug, J. Haegle, S. Biederer, T. F. Sattel, M. Erbe, R. L. Duschka, J. Barkhausen, and F. M. Vogt. Comparison of commercial iron oxide-based mri contrast agents with synthesized high-performance mpi tracers. *Biomed. Tech. / Biomed. Eng.*, 58(6):527–533, 2013. doi:10.1515/bmt-2012-0059.
- [3] R. Hufschmid, H. Arami, R. M. Ferguson, M. Gonzales, E. Tee-man, L. N. Brush, N. D. Browning, and K. M. Krishnan. Synthesis of phase-pure and monodisperse iron oxide nanoparticles by thermal decomposition. *Nanoscale*, 7(25):11142–11154, 2015. doi:10.1039/C5NR01651G.
- [4] N. Gehrke, A. Briel, F. Ludwig, H. Remmer, T. Wawrzik, and S. Wellert. New perspectives for mpi: A toolbox for tracer research. In *Springer Proceedings in Physics*, volume 140, pages 99–103, 2015. doi:10.1007/978-3-642-24133-8_16.
- [5] A. Kraupner, D. Heinke, R. Uebe, D. Eberbeck, N. Gehrke, D. Schüler, and A. Briel. Bacterial magnetosomes as a new type of biogenic mpi tracers. In *IWMPI*, pages 141–142, 2014.
- [6] D. Faivre and D. Schüler. Magnetostatic bacteria and magnetosomes. *Chem. Rev.*, 108(11):4875–4898, 2008. doi:10.1021/cr078258w.
- [7] C. Lang, D. Schüler, and D. Faivre. Synthesis of magnetite nanoparticles for bio- and nanotechnology: Genetic engineering and biomimetics of bacterial magnetosomes. *Macromol. Biosci.*, 7(2):144–151, 2007. doi:10.1002/mabi.200600235.
- [8] H. K. Henisch. *Crystals in Gels and Liesegang Rings*. Cambridge University Press, Cambridge, 2005. doi:10.1017/CBO9780511525223.
- [9] R. Prozorov, T. Prozorov, S. K. Mallapragada, B. Narasimhan, T. J. Williams, and D. A. Bazylinski. Magnetic irreversibility and the verwey transition in nanocrystalline bacterial magnetite. *Phys. Rev. B*, 76(5):054406, 2007. doi:10.1103/PhysRevB.76.054406.
- [10] J. Baumgartner, A. Dey, P. H. H. Bomans, C. Le Coadou, P. Fratzl, N. A. J. M. Sommerdijk, and D. Faivre. Nucleation and growth of magnetite from solution. *Nat. Mater.*, 12(4):310–314, 2013. doi:10.1038/nmat3558.
- [11] S. Laurent, D. Forge, M. Prot, A. Roch, C. Robic, L. V. Elst, and R. N. Muller. Magnetic iron oxide nanoparticles: Synthesis, stabilization, vectorization, physicochemical characterizations, and biological applications. *Chem. Rev.*, 108(6):2064–2110, 2008. doi:10.1021/cr068445e.